Neuropharmacology 144 (2019) 172–183

Contents lists available at ScienceDirect

Neuropharmacology

journal homepage: www.elsevier.com/locate/neuropharm

Amphetamine enantiomers inhibit homomeric α7 nicotinic receptor through a competitive mechanism and within the intoxication levels in humans

Daniel R. Garton[a,1], Sharmaine G. Ross[b], Rafael Maldonado-Hernández[c], Matthias Quick[d], José A. Lasalde-Dominicci[e,f], José E. Lizardi-Ortiz[f,g,*,2]

[a] Columbia College of Columbia University, New York, NY, 10027, USA
[b] Department of Biobehavioral Sciences, Teachers College Columbia University, New York, NY, 10027, USA
[c] Department of Biology, University of Puerto Rico, Río Piedras Campus, San Juan, PR, 00931, USA
[d] Department of Psychiatry, Molecular Therapeutics Division, Columbia University Medical Center, New York, NY, 10032, USA
[e] Departments of Biology and Chemistry, University of Puerto Rico, Río Piedras Campus, San Juan, PR, 00931, USA
[f] Molecular Sciences Research Center, University of Puerto Rico, San Juan, PR, 00927, USA
[g] Departments of Neurology and Psychiatry, Columbia University Medical Center, New York, NY, 10032, USA

HIGHLIGHTS

- Amphetamine competitively inhibits α7 nicotinic receptors at physiological levels.
- Amphetamine binding site localization is directed by hydrogen bonding to Ser144.
- α7 receptor full knock-out mice display altered behavioral response to amphetamine.
- The α7 receptor could be a potential target for treatment of AMPH abuse.

ARTICLE INFO

Keywords:
Alpha 7 nicotinic acetylcholine receptor
Amphetamine-type stimulant
Pharmacological characterization
In silico docking analysis
Amphetamine-induced locomotion
Alpha 7 upregulation

ABSTRACT:

Amphetamine-type stimulants (ATS) are the second most consumed illicit drug worldwide and lack good treatments for associated substance use disorders, lagging behind other addictive drugs. For this reason, a deeper understanding of the pharmacodynamics of ATS is required. The present study seeks to determine amphetamine (AMPH) enantiomers' effects on the homomeric α7 nicotinic acetylcholine receptor (α7 nAChR). Here we have shown that AMPH enantiomers bind to the α7 nAChR and competitively inhibit acetylcholine responses. Our *in silico* docking analysis suggests that AMPH binds close to the β7 strand of the B-loop of a chimera comprising of the human α7 nAChR and the acetylcholine binding protein from *Lymnaea stagnalis*. This may inhibit the required movement of the C-loop for channel opening, due to steric hindrance, providing a structural mechanism for its antagonist effect. Finally, we have shown that, in α7 nAChR full knockout mice, the behavioral response to D-AMPH is attenuated, providing direct evidence for the role of α7 nAChRs on the physiological response to D-AMPH. Importantly, D-AMPH exerts these effects at concentrations predicted to be pharmacologically relevant for chronic methamphetamine users and during binges. In conclusion, our data present new findings that implicate the α7 nAChR on the pharmacodynamics of ATS, which may be important for behavioral responses to these drugs, indicating a potential role for α7 nAChRs in ATS substance-use disorders.

Abbreviations: ATS, Amphetamine-type stimulants; METH, methamphetamine; nAChR, nicotinic acetylcholine receptor; AMPH, amphetamine; MDMA, 3,4-methylenedioxymethamphetamine; ACh, acetylcholine; MLA, methyllycaconitine; MPEA, 1-methyl-2-pyridin-3-ylethylamine; AChBP, acetylcholine binding protein; hα7R, human α7 nicotinic receptor; mα7R, mouse α7 nicotinic receptor; RMSD, root-mean-square deviation

* Corresponding author. Molecular Sciences Research Center, University of Puerto Rico, 1390 Ave. Ponce de León, Floor 2, San Juan, PR, 00927, USA.
E-mail address: jelizardiortiz@gmail.com (J.E. Lizardi-Ortiz).
[1] Present Address: Doctoral Programme Brain and Mind, University of Helsinki, Fabianinkatu 33, 00014, Helsinki, Finland.
[2] Present Address: Institute of Neurobiology, University of Puerto Rico, San Juan, PR 00901, USA.

https://doi.org/10.1016/j.neuropharm.2018.10.032
Received 8 June 2018; Received in revised form 10 October 2018; Accepted 21 October 2018
Available online 23 October 2018

1. Introduction

Amphetamine-type stimulants (ATS) are a family of psychoactive drugs that contain a substituted α-methylated phenethylamine backbone and mainly exert their physiological effects by reversing monoamine transporters. Depending on their substituent groups, pharmacology, and behavioral responses, they have been classified into three different classes known as the amphetamine, the cathinone, and the mescaline class (mescaline itself is a non-α-methylated phenethylamine and not considered an ATS; Cao et al., 2016; Sulzer et al., 2005).

In the past decade, ATS have become the second most consumed illicit drugs worldwide after marijuana (United Nations Office on Drugs and Crime, 2016). In the United States, a 2016 survey has reported that ATS are the third most consumed illicit drugs among adolescents and adults (12 years or older) after marijuana and pain relievers (Center for Behavioral Health Statistics and Quality, 2017). However, among adolescents and adults younger than 23, ATS misuse ranks second with prevalence ranging from 1.0% to 9.4%, and the prevalence is even higher (~11.1%) among male college students (Miech et al., 2017; Schulenberg et al., 2017). This clearly departs from the prevalence observed for other illicit drugs, including nonheroin narcotics (0.8%–5.8%; college students ~6.1%) and cocaine (0.8%–6.6%; college students ~6.3%). Consequently, ATS pose serious implications for public health due to the correlation between recreational drug use during adolescence and the higher likelihood of developing personal, social, and health problems, including substance use disorders, during adulthood (Winters et al., 2014).

Unfortunately, treatments for ATS addiction have lagged in comparison to treatments for alcohol, nicotine, and opioids due to the lack of effective pharmacotherapies (Cao et al., 2016). Bupropion, a monoamine transporter inhibitor of the cathinone class, is currently considered the most effective therapeutic drug for methamphetamine abusers (METH, the N-methylated analog of amphetamine; Elkashef et al., 2008). Interestingly, bupropion also inhibits α3β2, α4β2, and α7 nicotinic acetylcholine receptors (nAChRs) through a noncompetitive mechanism (Slemmer et al., 2000). Bupropion potency on β2-containing nAChRs (2–10 μM) lies within the potency for dopamine and norepinephrine transporters, pointing out the importance of nAChRs in bupropion pharmacotherapy (Musso et al., 1993; Slemmer et al., 2000).

Moreover, binding and cellular studies have also shown that nAChRs are targeted by other ATS, including amphetamine and 3,4-methylenedioxymethamphetamine (MDMA), a mescaline-class ATS (Chipana et al., 2008; Liu et al., 2003; Spitzmaul et al., 1999). Collectively, these studies have provided enough evidence to conclude that some ATS may bind to nAChRs. However, they fall short from the extensive pharmacological characterization that is required for rationalizing possible physiological consequences on animal models or humans.

In this study, we assessed the pharmacological action of AMPH enantiomers on the α7 nAChR and its behavioral effect. Our results demonstrate AMPH competitively inhibits α7 nAChRs and that this effect may arise from its location within the acetylcholine (ACh) binding pocket. But more remarkably, AMPH potency overlaps with blood levels (7.5–28.8 μM) attained after a typical recreational dose (0.25–1 g; Tallóczy et al., 2008). Furthermore, our behavioral results provide evidence that the α7 nAChR is an important element in the D-AMPH-induced locomotor response. In conclusion, this work supports a strong link between AMPH and α7 nAChRs, thus, proposing nAChRs as potential targets for refining the pharmacotherapeutic strategies for treating chronic AMPH/METH abuse.

2. Materials and methods

For detailed information about materials, methods, and procedures, see Supplementary Methods.

2.1. Drugs and reagents

All salts and reagents were ACS grade and purchased from Fisher Scientifics (www.fishersci.com), Sigma-Aldrich (www.sigmaaldrich.com), and Tocris Biosciences (www.tocris.com). [^{3}H]-methyllycaconitine (100 Ci/mmol in ethanol/water) from American Radiolabeled Chemicals (www.arcincusa.com); methyllycaconitine citrate from Tocris Biosciences (www.tocris.com); D-amphetamine hemisulfate was purchase from Sigma-Aldrich; L-amphetamine hydrochloride from Lipomed Inc (www.lipomed.com); and (±)-1-methyl-2-pyridin-3-ylethylamine from Broadpharm (www.broadpharm.com). Antibodies for tyrosine hydroxylase and the dopamine transporter were purchased from EMD Millipore (www.emdmillipore.com). *Xenopus laevis* oocytes were obtained from EcoCyte Bioscience (www.ecocyte-us.com).

2.2. Animals

C57BL6/J and α7 nAChR full knockout (B6.129S7-Chrna7^{tm1Bay}/J) mouse lines were purchased from the Jackson Laboratory (Bar Harbor, ME, USA). Mice were housed under a normal light cycle (12 h light/dark cycle) and standard conditions with food and water ad libitum. Wild type neonates (P0—P2) were used for preparing primary neuronal cultures and young adult mice (8–12 weeks old) were used for open-field and binding experiments. All experiments and procedures were performed in accordance to the Institutional Animal Care and Use Committees of Columbia University, National Institute of Health, and institutional guidelines.

2.3. [^{3}H]-methyllycaconitine (MLA) binding assays

Competition and upregulation experiments were evaluated in triplicate and each replicate comprised tissue from five C57BL6/J mice. P2 membrane preparations (100 μg total protein) were diluted to a final volume of 50 μl in modified PBS and incubated for 2 h on ice. Nonspecific binding was determined by preincubating unlabeled MLA (1 μM) for 1 h. Incubation was completed by rapid filtration under a vacuum and washed 3 times with ice-cold PBS.

Competition assays were performed on hippocampal preparations by adding 1.5 nM [^{3}H]-MLA in the presence of D-AMPH (0, 0.1, 1, 10, 100, and 1000 μM). Data points were calculated as [^{3}H]-MLA fmol/mg total protein and normalized against D-AMPH at 0 μM. The displacement curve was fitted to a homogeneous one binding site model. The K_D value for MLA was 0.45 nM. Upregulation experiments were performed on prefrontal cortex, striatal, and hippocampal preparations from saline- and D-AMPH-treated mice (2.0 mg/kg, twice a day for 10 days). Samples were incubated with 10 nM [^{3}H]-MLA, and data points presented as [^{3}H]-MLA fmol/mg total protein.

2.4. Two-electrode voltage clamp in Xenopus laevis oocytes

Human α7 cRNA (80 ng) was injected into oocytes and incubated for 96–120 h. All drugs were diluted in MOR-2 (external solution). Recordings were performed at room temperature and holding potential was clamped at −70 mV. Expression was verified by an ACh pulse ("Normalizing Pulse", 5 s, 1 mM). Recordings with basal currents smaller than 100 pA and ACh responses bigger than 300 pA were selected for analysis. A minimum of five oocytes were analyzed per drug.

Concentration − Response Curves: To test agonism, increasing concentration pulses (5 s; 0, 1, 3, 10, 30, 100, 300, and 1000 μM) of ACh, D- or L-AMPH, and 1-methyl-2-pyridin-3-ylethylamine ((±)-MPEA) were used. To test antagonism, a preincubation pulse (5 s) with increasing concentrations of D- or L-AMPH (0, 0.1, 1, 10, 100, and 300 μM) were followed by ACh (1 mM) + AMPH coperfusion. Response magnitude was obtained by calculating the net charge (area under the curve) and normalized against the "Normalizing Pulse". EC_{50} and IC_{50} were determined from the fitted equation Y = BOTTOM + (TOP -

BOTTOM)/[1 + $10^{(Log\ C\_X)\ \cdot\ Hill\ Slope)}$].

Current−Voltage (IV) Relationship: Drug pulses lasted 22 s and a step ramp from −100 to +60 mV (Δ20 mV, 800 ms/step) was applied 10 s after pulse onset. A nondesensitizing ACh concentration (55 μM) was perfused alone or in combination with D- or L-AMPH (30 μM). Current magnitude was determined by subtracting the last 200 ms of each step during MOR-2 perfusion from the ACh perfusion or ACh + D or L-AMPH coperfusion. Current magnitude was normalized against the current at −70 mV.

2.5. Whole-cell voltage clamp in primary neuronal cultures from the CA1 region of the hippocampus

Coverslips containing primary cultures (10–12 days in vitro) from the CA1 region of C57BL6/J mice were perfused with modified HEPES-buffered Tyrode's solution (mHBTS containing DNQX, gabazine, atropine sulfate) at room temperature. All drugs were diluted in mHBTS. Voltage was clamped at −70 mV and series resistance compensated to 70%. α7 nAChR currents were initially selected by shape and confirmed at the end using MLA (10 nM). Recordings with ACh responses bigger than 50 pA and basal currents smaller than 75 pA were selected for analysis.

Concentration−response curve: Responses were induced by applying 2 mM ACh through a puffing pipette (16 psi, 150 ms). The puffing pipette was placed ~25 μm away (diagonal) from neurons. To test agonism, a second puffing pipette containing 2 mM D- or L-AMPH was used. To test antagonism, concentrations of D- or L-AMPH (0, 2.2, 22, 220, and 730 μM) were perfused in the bath while ACh was puffed every minute. Basal response was determined using five ACh prepulses. Then, the drug was applied during the next five pulses, followed by a wash period of 10 pulses (Supplementary Fig. 2C and D). Only one neuron was screened per concentration, and a minimum of three cells were used per concentration. Response magnitude was obtained by calculating the net charge and normalizing against the averaged basal response net charge. IC_{50} was determined from the fitted equation: Y = BOTTOM + (TOP - BOTTOM)/[1 + $10^{(Log\ C\_X)\ \cdot\ Hill\ Slope)}$].

Competition experiments: Solutions were applied for 2 s using a three-barrel stepper system. The barrels were placed ~500 μm away (diagonal) from neurons. Each ACh concentration (0.03, 0.3, or 3 mM) was evaluated against increasing D-AMPH concentrations (ACh + D-AMPH at 16, 87, or 200 μM). Percent D-AMPH-induced inhibition for each ACh concentration was calculated via the difference between ACh net charge and ACh + D-AMPH normalized to ACh net charge. Data points were presented as mean ± SEM and a minimum of four neurons were analyzed per condition.

2.6. In silico docking analysis

Analysis was performed using the Autodock 4.2 program suite. A chimera comprising the human α7 nAChR and the *Lymnaea stagnalis* acetylcholine binding protein (AChBP) resolved by Li et al., (2011) (α7/AChBP; PDB entry: 3sq9) was used. Docking was performed on dimers formed by subunits A and B of the Apo conformation. The water bridging Leu104 and Leu116 was added by superimposing the *L. stagnalis* AChBP "Apo" structure resolved by Celie et al., (2004). All polar hydrogens were added to the α7/AChBP and a formal charge of +1 was added to the amine group of the ligands by protonation.

Ligands were docked using default Autogrid and Autodock settings. Flexibility of the residues shaping the nicotine binding site was included. Default settings were used for generating an 8000 $Å^3$ cubic grid that was centered at Trp145's indole nitrogen. 100 points (0.2 Å between points) were used in each direction to encompass the whole binding site and to leave enough space to allow docking outside of the binding site. The whole docking procedure was independently run 10 times. The amount of orientations per run was chosen based on the run that has less orientations before reaching the differentiation criteria (binding energy standard error limit: 2.5 kcal/mol). For clustering, root mean square deviations from all possible pairs and coordinates for ligand amine nitrogen and phenyl C4 carbon positions (120 conformations x 126 parameters matrix) were analyzed in Igor 6.0 using the farthest-point clustering algorithms. The same clustering analysis was performed by only using the amine nitrogen coordinates. Orientations were subsequently analyzed for intermolecular interactions with the α7/AChBP at a cut-off distance of 3.9 Å.

2.7. Open field paradigm

α7 nAChR wild-type and full knockout littermates were selected by specific genotyping procedures for this line (Jackson Laboratory website) and transferred to a satellite room (reversed light cycle) at least two weeks before experiments. The open field was a clear acrylic square box with white floor (43.5 × 43.5 × 30.5 cm) with two levels of infrared motion sensors. Interruptions of at least four consecutive beams within less than half a second was recorded as a movement score. Cumulative counts were compiled and downloaded every minute. Mice were daily handled for 5 min and injected with saline (0.9% NaCl) during the preceding four days to reduce stress. Mice were habituated to protocol conditions on days five and six by transferring them to the open field box and monitoring locomotion for 1.5 h, followed by a saline injection and another 1.5 h of monitoring. On the seventh day, the same paradigm was used, but mice received a D-AMPH injection (1.5 mg/kg). The time length used for calculating total locomotion was defined as the time that it takes to all genotypes to reach the same locomotion level after D-AMPH injection (70 min).

3. Results

3.1. D-AMPH displaces [^{3}H]-Methyllycaconitine

We first corroborated D-AMPH competitive binding on α7 nAChRs by performing a [^{3}H]-MLA competition binding assay under equilibrium conditions on hippocampal tissue (Fig. 1A). We found D-AMPH displaced [^{3}H]-MLA with an inhibition constant (K_i) of 49.7 μM (95% C.I.: 6.6–375 μM). Furthermore, bound [^{3}H]-MLA levels at the highest D-AMPH concentration (1 mM) was reduced to 6.5 ± 8.9% of the total binding level, agreeing with a practically total [^{3}H]-MLA displacement.

3.2. AMPH enantiomers inhibit the human α7 nicotinic receptor

We analyzed AMPH enantiomer potencies on the human α7 nAChR (hα7R) expressed on *Xenopus laevis* oocytes through electrophysiological methods. In voltage clamp experiments, ACh perfusion resulted in a concentration-dependent hα7R activation, but no activation was detectable by any of the enantiomers, ruling out agonism on hα7R (Fig. 1B, EC_{50}: 96.0 μM, 95% C.I.: 82–113 μM). Next, we evaluated hα7R inhibition by pre-perfusing the enantiomer before ACh/enantiomer coperfusion. Both enantiomers produced a concentration-dependent reduction in ACh-induced response, with a small but significant difference in potencies (Fig. 1C; D-AMPH: IC_{50}: 3.2 μM, 95% C.I.: 1.7–6.2 μM; L-AMPH: 11.7 μM, 95% C.I.: 6.6–20.6 μM; extra sum−of−squares F test for potency, P = 0.005).

3.3. AMPH enantiomers are not open channel blockers

We assessed whether AMPH enantiomers are open channel blockers. In current−voltage (I−V) relationships, nAChRs show rectification at negative potentials in the presence of cationic channel blockers. Neither enantiomer rectified the I−V curves at negative potentials, ruling out this mechanism (Fig. 1D; ACh: 55 μM; D-AMPH: 30 μM, two-way ANOVA, treatment P = 0.37; L-AMPH: 30 μM, two-way ANOVA, treatment P = 0.64).

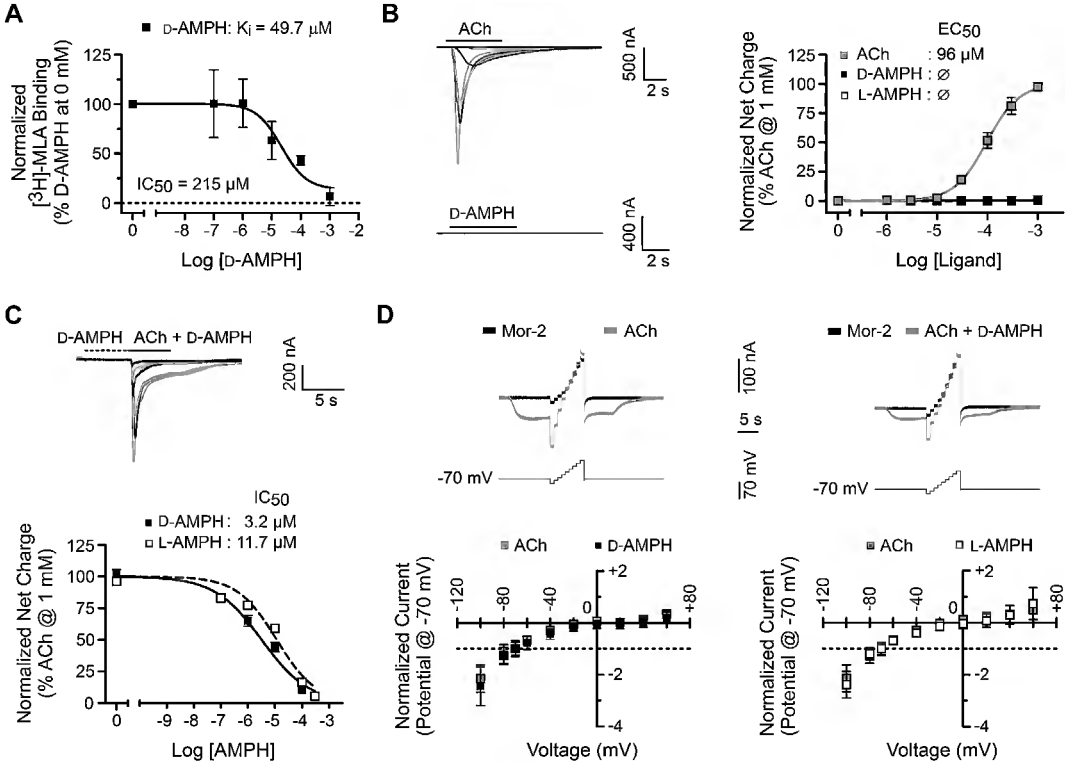

Fig. 1. Amphetamine enantiomers inhibit α7 nAChRs through a competitive mechanism. **A**. [^{3}H]-MLA competition binding assay on hippocampal tissue. Binding experiments were performed on ice (n = 3), and the inhibition constant (K_i) calculation model was fitted to a single binding site model using a K_D of 0.45 nM for MLA. D-AMPH displaces [^{3}H]-MLA (1.5 nM) in a concentration-dependent manner, reaching levels close to [^{3}H]-MLA nonspecific binding at the highest D-AMPH concentration. **B**. Concentration − response curve for hα7R activation by ACh (1–1000 µM) and AMPH enantiomers (3–1000 µM) *Left*: Representative traces for hα7R macroscopic currents generated by ACh and D-AMPH on *Xenopus laevis* oocytes. ACh or D-AMPH were perfused for 5 s. Traces alternate in color (grey and black) for visual facilitation. *Right*: ACh induces hα7R currents (n = 5) in a concentration-dependent manner, while each enantiomer displays no responses (n = 8). **C**. Concentration − response curve for hα7R inhibition by AMPH enantiomers. *Top*: Representative traces for hα7R macroscopic currents generated by ACh and D-AMPH. Antagonism was tested by pre-perfusing the respective enantiomers (0.1–300 µM, 5 s), followed by ACh (1 mM) + AMPH coperfusion (5 s). *Bottom*: AMPH enantiomers inhibit hα7R currents with significantly different potencies. Extra sum − of − squares F test, F(1,115) = 8.4, P = 0.005. **D**. Current − voltage (IV) relationship for hα7R inhibition by AMPH enantiomers. *Top*: Representative traces for the voltage ramp applied during ACh (55 µM) and ACh + D-AMPH (30 µM) coperfusion. A nondesensitizing ACh concentration was perfused with or without the respective AMPH enantiomer for 22 s. The ramp was applied 10 s after ligand exchange onset. *Bottom*: AMPH enantiomers do not rectified the IV relationship at negative potentials as expected for open channel blockers (D-AMPH: n = 5–6, two-way ANOVA, treatment F(1,90) = 0.82, P = 0.37; L-AMPH: n = 6, two-way ANOVA, treatment F(1,100) = 0.22, P = 0.64). Each data point is represented as mean ± SEM.

3.4. AMPH enantiomers competitively inhibit the mouse α7 nicotinic receptor in primary neuronal cultures from the CA1 region of the hippocampus

We performed whole-cell voltage clamp on the type I, methyllycaconitine (MLA)-sensitive mouse α7 nAChR (mα7R) from primary cultures of the CA1 region aiming to confirm AMPH's pharmacological properties in a neuronal environment. To assess whether the enantiomers could trigger intracellular mechanisms that may indirectly modulate mα7R in this culture, we first searched for catecholamine markers and Ca^{2+} signaling. This culture shows no catecholamine synthesis or plasmalemmal dopamine transporter (DAT), as reflected by the absence of tyrosine hydroxylase and DAT immunofluorescence labeling on neurons (Supplementary Fig. 1A) and glia (data not shown) from wild type mouse (WT) cultures. We also attempted norepinephrine transporter immunolabeling, but signal/noise ratio from all tested antibodies was not large enough to produce a reliable detection in cultures from locus coeruleus (data not shown). Changes in intracellular Ca^{2+} levels were analyzed by bath perfusing D- or L-AMPH on cultures obtained from GCaMP3–Nestin CRE mice. No significant changes, except for L-AMPH at 2.2 µM, were detected in mα7R-expressing neurons (Supplementary Fig. 1B, and C), mα7R-nonexpressing neurons (data not shown), and glia (data not shown). These results argue against a potential mα7R modulation by Ca^{2+} or catecholamine signaling in this culture.

Nonetheless, voltage clamp experiments for estimating AMPH IC_{50} values in cultures from WT mice displayed a sustained and reversible hyperpolarizing change in basal current (a shift in trace's baseline current to smaller negative values) during AMPH perfusions at high concentrations. (Supplementary Fig. 2A; 220 µM: 10.8 ± 2.4 pA, 730 µM: 16.6 ± 3.5 pA; one-way ANOVA, P = 0.007; Dunnett's posttest: 0 vs 220 µM and 0 vs 730 µM, P < 0.05). This hyperpolarizing current was also observed at high D-AMPH concentrations during competition experiments. However, this current probably reflects an unknown and independent K^+ or Cl^- conductance that could affect the analysis of the ACh-induced responses depending on the employed protocol for drug delivery, as is explained below for each case.

Then, we analyzed whether AMPH enantiomers activate the mα7R in WT cultures. The mα7R-positive neurons were recognized by fast-kinetics responses produced by ACh and confirmed at the end of each experiment with 10 nM MLA (Fig. 2A and Supplementary Fig. 2B). Neither enantiomer (up to 1 mM) induced mα7R responses when applied through the puffing pipette (data not shown), agreeing with the lack of responsiveness displayed by the hα7R. Next, we evaluated the inhibition potencies by bath perfusing each enantiomer while puffing ACh. As observed with the hα7R, AMPH enantiomers produced a concentration-dependent inhibition, but in contrast to hα7R, potencies were not significantly different (Fig. 2A and Supplementary Fig. 2C and

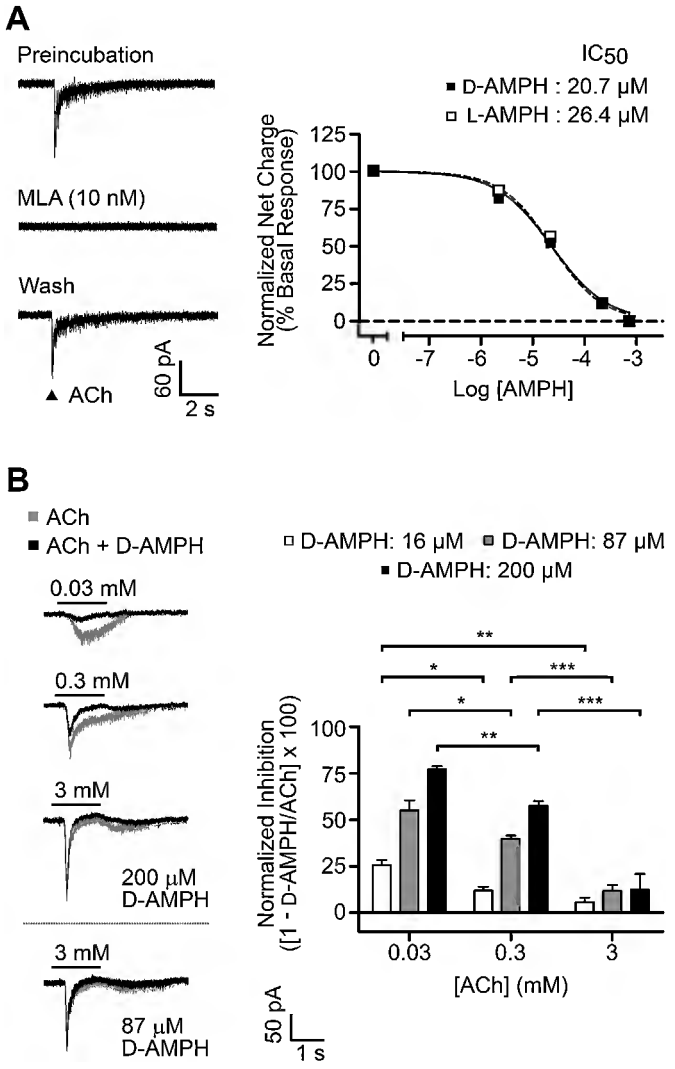

Fig. 2. D-Amphetamine displays surmountable inhibition on α7 nAChR endogenously expressed in primary cultures from the CA1 region of the hippocampus. **A**. Concentration − response curve for mα7R inhibition by AMPH enantiomers. *Left*: Representative traces for MLA-sensitive, mα7R macroscopic currents recorded from primary cultures of the CA1 region. ACh (2 mM) was air-pressured applied (150 ms, 16 p.s.i.; arrowhead) through a glass micropipette (1–2 µm tip) 20 µm away from the neuron. *Right*: AMPH enantiomers inhibit mα7R currents with no differences in potencies. Extra sum − of − squares F test, $F(1,42) = 2.8$, $P = 0.1$, $n = 3$–5 cells/concentration. A $n = 3$ was only used for L-AMPH at 730 µM, which displayed total mα7R inhibition like D-AMPH at 730 µM ($n = 5$) and experiments in oocytes for the hα7R. Antagonism was tested by bath applying one of the enantiomers (0–730 µM, 10 min), while ACh was air-pressured puffed every minute. **B**. ACh vs D-AMPH competition analysis. *Left*: Representative traces for mα7R currents. ACh, D-AMPH, and ACh + D-AMPH solutions were rapidly exchanged (~20 ms) by a fast perfusion system, and cells were perfused for 2 s. *Right*: Increasing ACh concentrations reduce D-AMPH inhibition until reaching a concentration with minimal inhibition (two-way ANOVA, interaction $F(4,33) = 11.0$, $P = 0.0001$; Fisher's LSD posttest, *$P < 0.05$, **$P < 0.01$, ***$P < 0.001$; $n = 4$–5 cells/condition). D-AMPH concentrations represents the IC_{33}, IC_{66}, and IC_{90}. Each data point is represented as mean ± SEM.

D; D-AMPH IC_{50}: 20.7 µM, 95% C.I.: 16.5–26.0 µM; L-AMPH IC_{50}: 26.4 µM, 95% C.I.: 22.0–31.7 µM; extra sum − of − squares F test, $P = 0.10$). In this experiment, the hyperpolarizing current does not affect the IC_{50} estimation since it is present during the whole AMPH incubation period and is offset in the baseline subtraction step during net charge calculations.

Lastly, we used a fast-exchange perfusion system to provide further evidence about AMPH's inhibition mechanism by coperfusing ACh with D-AMPH at concentrations representing the IC_{33}, IC_{66}, and IC_{90} (Fig. 2B). In agreement with a competitive mechanism, increasing ACh concentration reduced D-AMPH inhibition until reaching a point (3 mM ACh) where minimal inhibition was achieved, consistent with a surmountable inhibitory mechanism (Fig. 2B; 0.03 mM ACh and D-AMPH, 16 µM: 25.6 ± 2.9%, 87 µM: 54.9 ± 5.5%, 200 µM: 77.2 ± 1.5%; 0.3 mM ACh + D-AMPH, 16 µM: 11.9 ± 2.1%, 87 µM: 39.6 ± 1.7%, 200 µM: 57.5 ± 2.5%; 3.0 mM ACh + D-AMPH, 16 µM: 5.7 ± 2.5%, 87 µM: 11.7 ± 3.1%, 200 µM: 12.5 ± 8.3%; two-way ANOVA, interaction $P = 0.0001$). However, traces recorded at 3 mM ACh (Figs. 2B, 87 and 200 µM D-AMPH) showed that the D-AMPH-triggered hyperpolarizing current affects the normalized inhibition. This current possibly become evident at 3 mM due to mα7R desensitization, and its presence in the D-AMPH + ACh traces is denoted by a hyperpolarized phase with respect to the baseline (the area under the curve becomes positive with respect to the baseline). We did not observe this current at 16 µM D-AMPH, agreeing with the data obtained at 22 µM D-AMPH for the IC_{50} estimation. On the other hand, it counteracts the response of uninhibited mα7Rs at 87 and 200 µM D-AMPH. Analysis of the hyperpolarized phase showed that this could account for ~4% and 6% of the total net charge for D-AMPH at 87 and 200 µM, respectively.

3.5. D-AMPH binding to the α7/acetylcholine binding protein (α7/AChBP) chimera is possibly stabilized by concurrent hydrogen bonds with serine 144's carbonyl group and tyrosine 91's hydroxyl group and aromatic interactions

To unveil the interactions stabilizing D-AMPH binding, we performed *in silico* docking analyses using the crystal structure from a chimera comprising the hα7R and *Lymnaea stagnalis* AChBP (Supplementary Fig. 3A; Li et al., 2011). The center of the docking volume (8000 $Å^3$ cube) was superimposed over Trp145 (Fig. 3A), which displays the same orientation in Apo and epibatidine-bound conformations. The water molecule bridging residues Leu104 and Leu116 (Fig. 3C and Supplementary Fig. 3B) was included in the analysis by superimposing the β5 − β6 sheets from the α7/AChBP with the same segment on the "Apo" conformation of the *L. stagnalis* AChBP resolved by Celie et al. (2004).

The docking analysis was performed using flexible side chain conditions on the α7/AChBP Apo conformation. The analysis was run ten times (25 orientations/run) and the 12 most stable orientations from each run were selected (120 orientations in total). Differences in binding energies (−7.07 − −5.90 kcal/mol) were not large enough (ΔE = 2.5 kcal/mol) to select the most likely orientation. However, a clustering analysis using the root mean square deviation (RMSD) values from all possible pairs and docking coordinates for D-AMPH's nitrogen and C4 carbon segregated the conformations into 9 different clusters (Supplementary Fig. 3C and Supplementary Table 1). The most populated cluster (Cluster 7) held 38 out of 120 orientations, followed by clusters holding 27 (Cluster 4), 21 (Cluster 1), and 19 (Cluster 3) orientations. The rest of the clusters hold between 1 and 5 orientations. A scatterplot using cluster's mean binding energy and the number of orientations showed no correlation between these parameters, suggesting that big clusters are not energetically favored to occur (Supplementary Fig. 3C). Remarkably, the D-AMPH amine group tends to localize close to Ser144's carbonyl group. A second clustering analysis for D-AMPH's nitrogen coordinates showed that Clusters 1, 3, 7, and 8 (83 orientations for a 69% of the total) fall into the same nitrogen cluster (Fig. 3B and Supplementary Fig. 3D). The main difference among these clusters was the direction of the phenyl group within the ACh binding site (Supplementary Fig. 3E).

Cluster 8 was excluded from further analysis because, in contrast to the other clusters, most orientations only displayed one hydrogen bond that differently interact with either Ser144 or Trp145 and one showed

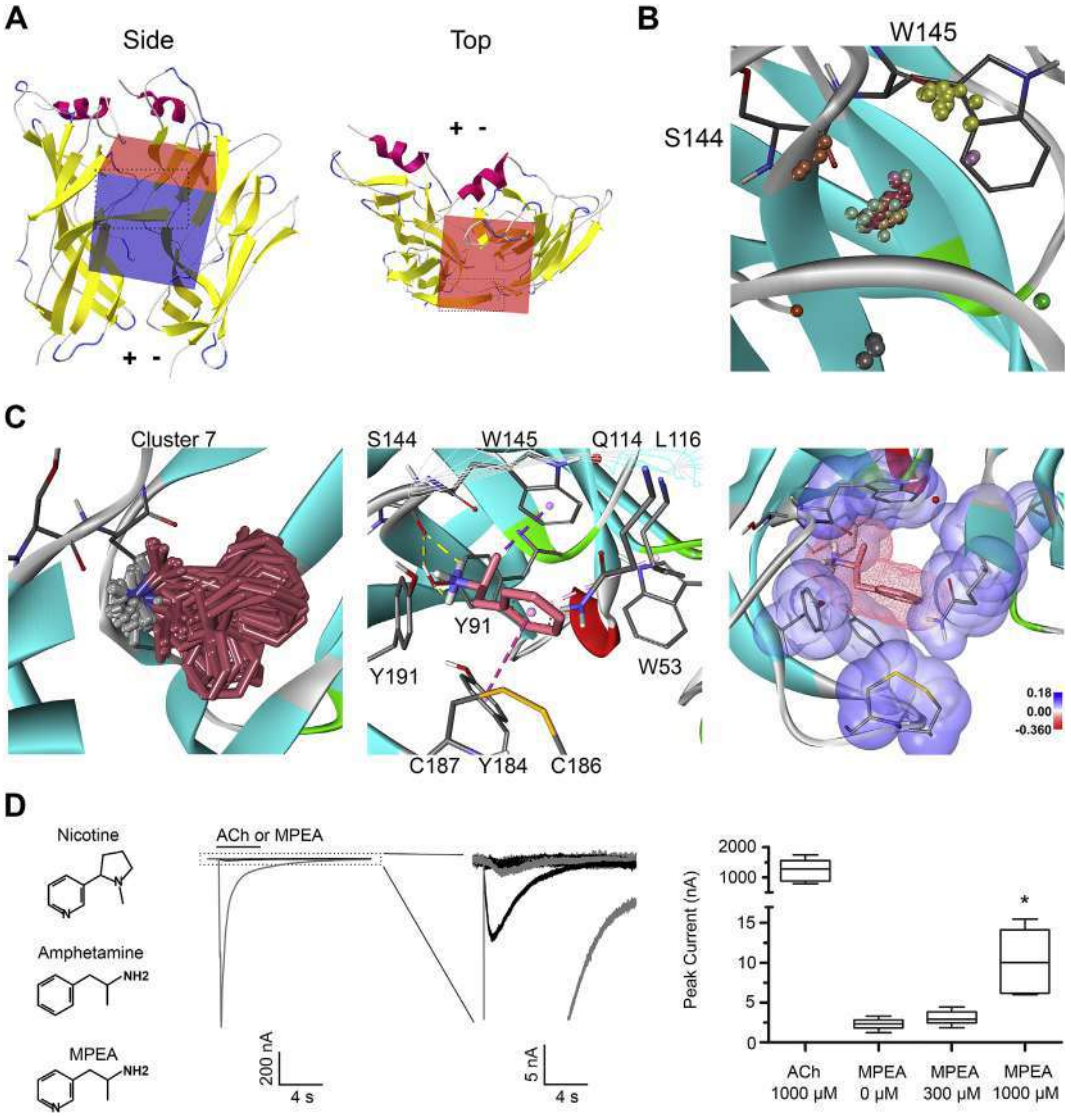

Fig. 3. D-Amphetamine binding to an α7/AChBP chimera is stabilized by hydrogen bonding to Ser144's backbone carbonyl groups. **A**. Side and top views for the volume of the α7/AChBP chimera binding site (cube) that was selected for docking analysis. The cube center was superimposed over Trp143 and the edge dimensions are 100 Å. The dotted box demarcates the β strands (β9 and β10) comprising the C-loop, and the + and – symbols signify the principal and complementary sides of the binding site. **B.** Nitrogen atoms from the D-AMPH molecules display a high degree of occurrence near Ser144's carbonyl group. The docking protocol was run ten times using the "Apo" α7/AChBP conformation, with residues delineating the nicotine binding site allowed to rotate freely, except for Trp145. Cluster 1: 21 orientations (mint green), Cluster 2: 4 orientations (dark grey), Cluster 3: 19 orientations (banana mania), Cluster 4: 27 orientations (yellow), Cluster 5: 1 orientation (green), Cluster 6: 1 orientation (orange), Cluster 7: 38 orientations (pink salmon), Cluster 8: 5 orientations (light violet), Cluster 9: 4 orientations (tangerine). **C**. Docked D-AMPH molecules residing close to the β7 strand of the B-loop may prevent C-loop displacement by steric hindrance. *Left*: Orientations from the most populated cluster, Cluster 7. Part of the C-loop was removed to improve visualization. *Center*: Orientations in Cluster 7 were stabilized by coincident hydrogen bonds with Tyr91 and Ser142. The orientation with the lowest root mean square (RMS, 1.95 Å, −6.09 kcal/mol) within this cluster is displayed. RMS for each orientation was calculated using the RMSD for each combination in the clusters. Dashed lines show hydrogen bonds with Tyr 91 and Ser142 (yellow), the π−σ interaction with Trp145 (purple), and the π−π stack interaction with Tyr184 (magenta). No interaction with water was observed. *Right*: van der Waals radius for the orientation with the lowest RMS. This orientation interacts (cutoff distance 3.9 Å) with all residues involved in nicotine binding, except Leu116. The contacts made by Tyr91, Trp145, Tyr184, and Tyr 191 may prevent the C-loop displacement required for channel opening. Scale: partial atom charge. **D**. 1-methyl-2-pyridin-3-ylethylamine is an α7 nAChR agonist with negligible efficacy. *Left*: Nicotine, (±)-AMPH, and (±)-MPEA structures. *Center*: Representative traces for hα7R macroscopic currents generated by ACh and (±)-MPEA on *Xenopus laevis* oocytes. Traces alternate in color (grey and black) for visual facilitation. *Right*: (±)-MPEA hardly induces macroscopic currents on hα7R. ACh (1 mM) and (±)-MPEA (0–1000 μM) were perfused for 4 s. The mean peak current was 1278 ± 131 nA for ACh. For (±)-MPEA: 2.33 ± 0.26 nA at 0 μM, 3.09 ± 0.34 nA at 300 μM, and 10.2 ± 1.3 nA at 1000 μM. One-way ANOVA: $F(5,41) = 25.4$, $P < 0.001$; Dunnett's posttest (control: 0 μM (±)-MPEA): *$P < 0.05$; $n = 8$ oocytes. Data points represent mean ± SEM.

coincident hydrogen bonds with Ser144 and Trp145 (Supplementary Fig. 3F). Conversely, Clusters 1, 3, and, 7 shared a common set of interactions (Fig. 3C and Supplementary Fig. 4). These clusters comprised 78 orientations and 21 of the 30 most stable orientations (top 25%), including nine of the first twelve orientations (top 10%). When D-AMPH−α7/AChBP contacts were evaluated at a cutoff distance of 3.9 Å, we found similarities to the contacts observed in the nicotine−AChBP structure (Celie et al., 2004). On the principal side, D-AMPH interacted with Tyr91, Trp145, and Tyr191 side chains in 100%, 94%, and 100% of the orientations, respectively. Furthermore, many orientations (73%) made contacts with Tyr184, a residue that does not interact with nicotine, with a similar percentage among clusters (71%, 78%, and 71% in Cluster 1, 3, and 7, respectively). Also contrasting

with nicotine, a minority of orientations interacted with key residues (principal side: Cys187, 15%; complementary side: Trp53, 37%; Gln114, 6%; Leu116, 41%) and the water molecule (18%). These interactions were also not evenly distributed among clusters, with Gln114, Leu116, C187, and water preferentially observed in Cluster 7 (100%, 84%, 92%, and 100% of the cases, respectively) and Trp53 evenly distributed between Cluster 3 and 7 (55% and 45% of the cases, respectively).

D-AMPH also made extensive contacts with Trp145's backbone atoms and Ser144's carbonyl group on the principal side that were not observed with nicotine. All 78 orientations in these clusters displayed hydrogen bonds (57 orientations with Tyr91, 70 with Ser144, and 4 with Trp145). Multiple hydrogen bonds were detected in 50 orientations, and coincident hydrogen bonds between D-AMPH's amine hydrogen with the Tyr91's hydroxyl and Ser144's carbonyl groups were observed in 48 orientations (13 in Cluster 1, 8 in Cluster 3, and 27 in Cluster 7; middle panels in Fig. 3C and Supplementary Fig. 4). Remarkably, a well-structured hydrogen bond network, as the one presented in Fig. 3C, was observed in 15 orientations (Cluster 1: 19%, Cluster 3: 21%, and Cluster 7: 18%).

In addition to hydrogen bonding, aromatic interactions were frequently observed between D-AMPH and residues shaping the principal side of the ACh binding site. Possible interactions that stabilized the D-AMPH − α7/AChBP complex include [1] π − π stacks and π − π T-shape interactions between the rings of Trp145, Tyr184, and Tyr191 and D-AMPH's phenyl ring. [2] π − sigma interactions between D-AMPH's α-methyl substituent and Trp145's indole ring. [3] cation − π interactions between D-AMPH's amine group and Tyr191's phenyl ring. Moreover, other interactions could be playing a minor role in stabilizing D-AMPH binding, including [1] π − π interactions with Trp53; [2] π − alkyl interactions between D-AMPH's phenyl ring and the methylene bridge of Gln114 and Cys187; and [3] π − sulfur interactions between D-AMPH's phenyl ring and C187's sulfur atom.

Interestingly, these clusters are tightly packed near the “hinge” between the β7 strand and C-loop (β9 and β10 strands; right panels in Fig. 3C and Supplementary Fig. 4). This packing may constrain C loop motion, which contributes to the pore opening mechanism (Law et al., 2005; Unwin and Fujiyoshi, 2012). We hypothesized that competitive ligands capable of forming a hydrogen bond with Ser144 may act as an antagonist. To provide evidence for this hypothesis, the nicotinoid pharmacophore was introduced into the AMPH backbone by converting AMPH's benzene ring into a pyridine ring (1-methyl-2-pyridin-3-ylethylamine, MPEA; Fig. 3D, left figure). In agreement with our hypothesis, docking analysis and voltage clamp experiments demonstrated that D-MPEA displays a similar docking pattern to D-AMPH, especially the amine groups (Supplementary Fig. 5A) and that (±)-MPEA activates the hα7R at the highest concentration with negligible efficiency (Fig. 3D; ACh, 1000 μM: 1278 ± 131 nA; (±)-MPEA, 0 μM: 2.33 ± 0.26 nA, 300 μM: 3.09 ± 0.34 nA, 1000 μM: 10.2 ± 1.3 nA; one-way ANOVA, $P < 0.001$; Dunnett's posttest: (±)-MPEA 0 μM vs 1000 μM, $P < 0.05$).

Parallel to D-AMPH, differences in binding energies (−7.09 − −5.46 kcal/mol) were not large enough to differentiate among orientations and clustering analysis segregated the conformations into 6 clusters (Supplementary Table 2). Cluster 1 was the most populated cluster (41 orientations), followed by Cluster 6 and 5 with 39 and 30 orientations, respectively, and the rest of the clusters holding between 1 and 6 orientations. Again, the scatterplot for cluster's mean binding energy versus number of orientations also suggested that big clusters are not energetically favorable to occur (Supplementary Fig. 5B), and clustering analysis using D-MPEA's nitrogen coordinates was used to select the most probable clusters. Clusters 1 and 6 were grouped into the same nitrogen cluster, close to Ser144's carbonyl group, and the main difference between them was the direction of the phenyl group (Supplementary Fig. 5B).

These two clusters also shared the same set of interactions that stabilized D-AMPH binding into the α7/AChBP chimera (Supplementary Fig. 5C). These clusters comprised 24 of the most stable orientations in the top 25%, and ten of the top 10%. At a cutoff distance of 3.9 Å, 96% of the orientations made contacts with the side chains of Tyr91, Trp145, and Tyr191 and 72% with Tyr184 in the principal side. D-MPEA also displayed a small amount of orientations interacting with Cys187 (13%) in the principal side, and with Trp53 (44%), Gln114 (10%), and Leu116(43%) in the complementary side. The water molecule did contact in 18% of the orientations. As observed with D-AMPH, these interactions were not evenly distributed among clusters. Interactions with Gln114, Cys187, and water were observed in Cluster 1 and with W53 in Cluster 6. Interactions with Leu116 were evenly distributed between clusters (Cluster 1: 53% and Cluster 6: 47% of the cases).

D-MPEA also made extensive contacts with Trp145's backbone atoms and Ser144's carbonyl group on the principal side. Clusters 1 and 6 displayed hydrogen bonds in 66 orientations and hydrogen bonding to Ser144's carbonyl group was observed in 65 orientations (Supplementary Fig. 5C). Multiple hydrogen bonds were detected in 42 orientations but, differing from D-AMPH docking, coincident hydrogen bonds were also observed with water and the side chains of Trp53 and Tyr191. Hydrogen bonding to water and these residues were made by the pyridine's nitrogen electron pair. However, the coincident hydrogen bonding between D-MPEA's amine hydrogens and the Tyr91's hydroxyl and Ser144's carbonyl groups was the most frequent (11 orientations). Other multiple hydrogen bond combinations with D-MPEA include Ser144/water (5 orientations), Ser144/Tyr191 (7 orientations), Ser144/Trp53 (6 orientations), and Tyr91/Ser144/Trp53 (7 orientations). Moreover, similar aromatic interactions to D-AMPH could also be involved in stabilizing D-MPEA binding, including [1] π − π interactions between the rings of Trp145, Tyr184, and Tyr191 and D-MPEA's phenyl ring; [2] π − sigma interactions between D-MPEA's α-methyl substituent and the rings of Trp145 and Tyr191; [3] cation − π interactions between D-MPEA's amine group and Tyr191's phenyl ring; and [4] π − alkyl interactions between D-MPEA's phenyl ring and the methylene bridge of Leu116.

3.6. Ablation of the CHRNA7 gene in mouse disrupts D-AMPH-induced locomotion

We assessed in vivo significance for AMPH − α7 nAChR interrelationship by evaluating two physiological processes: D-AMPH-induced locomotion and mα7R upregulation. We, first, evaluated whether CHRNA7 gene ablation modifies D-AMPH-induced locomotion in the open field paradigm. The α7 nAChR full knockout mouse (KO) displayed no changes in locomotion with respect to the WT during the habituation phase of the first experimental day (Fig. 4A; Horizontal (cm), WT: 12499 ± 679, KO: 11141 ± 694; Student's t-test: $P = 0.18$), suggesting no alteration in basal locomotion or exploratory behavior. Furthermore, all genotypes showed similar locomotion levels when they were injected with saline during the treatment phase of the second experimental day, providing further evidence that ablation of the CHRNA7 gene produces no changes in basal locomotion (Fig. 4B, Saline; WT: 5714 ± 845, KO: 4947 ± 643; Fisher's LSD posttest, $P = 0.80$). Conversely, D-AMPH treatment (1.5 mg/kg, i.p., third experimental day) induced a significant 107% increase in horizontal locomotion in the KO mouse, which was significantly less than the 208% increase in the wild-type mice (Fig. 4B; D-AMPH, WT: 17601 ± 3982, KO: 10271 ± 1556; repeated measure two-way ANOVA: treatment $P < 0.0001$, interaction $P = 0.06$; Fisher's LSD posttest, WT(saline) − WT(D-AMPH): $P = 0.0004$, KO(saline) − KO(D-AMPH): $P = 0.05$, WT(D-AMPH) − KO(D-AMPH): $P = 0.02$). Nevertheless, the change in horizontal locomotion concomitantly occurs with a reduction in vertical movement in both genotypes, in accordance with D-AMPH inducing its effects on both WT and α7 nAChR KO mice (Fig. 4C, vertical counts; saline, WT: 729 ± 147, KO: 609 ± 84; D-AMPH, WT: 261 ± 71, KO:

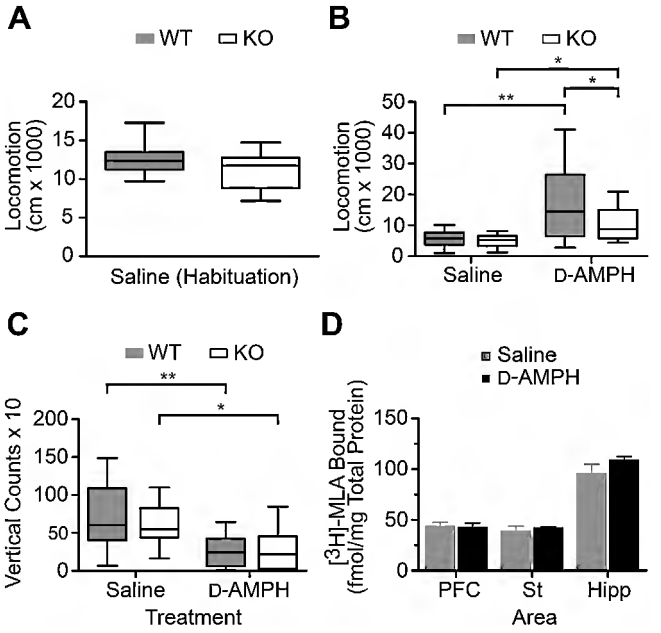

Fig. 4. D-amphetamine administration induces a reduced locomotion increase in α7 nAChR full knockout mice and does not upregulate α7 nicotinic receptors in wild type mice. **A.** α7 nAChR KO mice displays no changes in locomotion when exposed to an open field for the first time. Mice were acclimated to the chamber for 90 min (habituation phase), followed by the treatment injection and locomotion assessment for 90 min (treatment phase). The Box and Whisker graph covers the total data range. Habituation, WT: 12499 ± 679 (n = 10), KO: 11141 ± 694 (n = 12), Student's t-test P = 0.18. **B.** α7 nAChR KO mice displays reduced locomotion to an acute D-AMPH dose. Horizontal locomotion was assessed during the treatment phase with saline (second day) or D-AMPH (1.5 mg/kg, i.p., third day). motion. Saline, WT: 5714 ± 845, KO: 4947 ± 643; D-AMPH, WT: 17601 ± 3982, KO: 10271 ± 1556; two-way repeated measure ANOVA: treatment P < 0.0001, interaction P = 0.06; Fisher's LSD posttest: *P < 0.05, **P < 0.0005. **C.** Increase in horizontal locomotion concomitantly occurs with a reduction in vertical movement. Saline, WT: 729 ± 147, KO: 609 ± 84; D-AMPH, WT: 261 ± 71, KO: 257 ± 75; two-way repeated measure ANOVA: treatment P < 0.0001; Fisher's LSD posttest: *P < 0.01, **P < 0.005. **D.** D-AMPH does not modify α7 nAChR expression in the prefrontal cortex, striatum and hippocampus. Mice were injected twice per day with saline or D-AMPH (2.0 mg/kg, i.p.) for 10 days. α7 nAChR expression was assessed by [^{3}H]-MLA binding assay (10 nM) on ice. Bars represent mean ± SEM.

257 ± 75; repeated measure two-way ANOVA, treatment P < 0.0001; Fisher's LSD posttest, WT(saline) − WT(D-AMPH): P = 0.002, KO(saline) − KO(D-AMPH): P = 0.01).

3.7. D-AMPH does not induce upregulation of the mouse α7 nicotinic receptor in various brain areas

We investigated whether D-AMPH upregulates mα7R during an administration schedule that induces sensitization. We analyzed P2 membrane fractions from chronically treated WT mice using 10 nM [^{3}H]-MLA (Saline vs D-AMPH at 2 mg/kg, twice/day for 10 days). We found that D-AMPH induced no changes in [^{3}H]-MLA binding levels in the prefrontal cortex, striatum, and hippocampus (Fig. 4D, Saline vs D-AMPH (Student's t-test), prefrontal cortex: 43.7 ± 3.8 vs 42.5 ± 4.5 (P = 0.60), striatum: 38.7 ± 5.1 vs 42.1 ± 1.1 (P = 0.48), hippocampus: 95.8 ± 9.1 vs 108.8 ± 3.7 (P = 0.21)).

4. Discussion

Multiples studies have shown that ATS directly bind and modulate α7 and β2-containing nAChRs (Chipana et al., 2008; Liu et al., 2003; Spitzmaul et al., 1999). AMPH and MDMA displaced methyllycaconitine and epibatidine in mouse brain extracts at conditions imparting selectivity on α7 and heteromeric neuronal nAChRs, respectively. But, even though these drugs display no selectivity for nAChR subtypes, their pharmacological responses could be subtype-dependent. MDMA activates α7 nAChRs with low efficacy but blocks α4β2 in xenopus oocytes. D-AMPH induces Ca^{2+} influx through β2-containing and α7 nAChRs in chromaffin cells. However, a single channel study suggests D-AMPH is an open channel blocker of the muscle-type nAChR. These results, along with bupropion's noncompetitive mechanism, suggest that not all ATS share a common pharmacological mechanism on nAChRs and should be individually characterized.

In the present study, we studied AMPH, which holds the ATS prototypical structure and has similar pharmacokinetics, pharmacodynamics, and behavioral potency to METH, but has a higher prevalence among adolescent and young adults (Balster and Schuster, 1973; Hall et al., 2008; Lamb and Henningfield, 1994; Melega et al., 1995; Miech et al., 2017; Schulenberg et al., 2017). The α7 nAChR was selected because its homomeric assembly provides easy pharmacological interpretations by avoiding the complexity associated to heteromeric assembly, as observed in β2-containing receptor studies (Palma et al., 1996).

Our results contrast with the agonist mechanism proposed by Liu et al. (2003) in chromaffin cells. However, the increase in intracellular Ca^{2+} ($[Ca^{2+}]_i$) levels are also abolished by voltage-gated Ca^{2+} channel blockers, suggesting a more complex mechanism than just direct agonism. In contrast, our results were obtained from α7 nAChR expression systems that have been extensively used for pharmacological studies (Alkondon and Albuquerque, 1993; Palma et al., 1996). Two-electrode voltage clamp in oocytes provides the advantage of no endogenous expression of nAChRs and other receptors mediating AMPH effects. Thus, interpretation from primary cultures of the CA1 region could be limited by intracellular signals triggered by AMPH that modulate nAChR response, particularly phosphorylations and changes in $[Ca^{2+}]_i$ levels (Guo and Lester, 2007; Huganir et al., 1986). Our results suggest that our cultures lack proteins associated with dopamine synthesis and uptake, ruling out any mechanism related to dopamine signaling. Because these results agree with the hypothesis that monoamine synthesis and uptake are only mediated by their respective neurons, we suggest that primary cultures from the CA1 region are monoamine free. Following this hypothesis, AMPH's inability to modify $[Ca^{2+}]_i$ levels reflects deficiencies in monoamine transporters or absence of proteins that are necessary to trigger AMPH's effects.

However, a hyperpolarizing current was detected in primary cultures of the CA1 region that introduced an error of at least 4–6% in the analysis of the competition experiment at high D-AMPH concentrations. The fast on/off kinetics and sustained presence of this current probably reflects a receptor-mediated, K^+ or Cl^- conductance that still need to be identified and not a direct modulation of α7 nAChRs. AMPH is known to induce Na^+ and Cl^- conductances on monoamine transporters and the ligand-gated channel-55 (LGC-55), respectively (Sitte and Freissmuth, 2015). LGC-55 is an amine-gated channel related to the cys-loop superfamily, which include nAChR, $GABA_A$, and glycine receptors.

In oocytes, we found that D-AMPH blocks hα7Rs with a slightly higher potency than L-AMPH. Such differences, however, were not observed when the enantiomers were coperfused with ACh (no pretreatment, Supplementary Fig. 6) or in experiments performed on primary cultures from the CA1 region. In our experience, different oocyte batches usually display small differences in potency. Taken together, these data strongly suggest that both enantiomers inhibit α7 nAChR with same potency. Further evidence supporting our results comes from binding studies using nornicotine and 3-pyridyl ethers (Abreo et al., 1996; Copeland et al., 1991). These studies have shown that stereoselectivity is almost abolished when an amine's substituent groups are replaced by hydrogens. Therefore, we conclude that both isomers competitively inhibit α7 nAChRs with same potency within the low

micromolar range (1–30 μM).

The potency differences between the hα7R and mα7R probably arise from experimental designs. Sequence alignment shows high homology between their binding domains (~95% sequence identity) and no difference among residues delineating the binding pocket. Neuronal cultures offer the advantage of a native membrane and intracellular environment, which are known to regulate the nAChR gating mechanism (Hénault et al., 2015). Still, the drug delivery system used in this study may induce transient drug dilutions that could affect the results (Lopez-Hernandez et al., 2007). Conversely, while oocytes have the disadvantage of an amphibian environment, they provide an excellent solution exchange system.

Our data strongly suggest that both AMPH enantiomers competitively antagonize the α7 nAChR, based on D-AMPH competition results obtained from the [^{3}H]-MLA binding assay and electrophysiology. The hallmark of a competitive mechanism is a surmountable interaction. An insurmountable inhibition is usually concluded when the inhibitor could not completely displace a radioligand in binding experiments or when the maximal response produced by a high and saturating concentration of a ligand, in our case ACh, could not be achieved. In our binding experiments, [^{3}H]-MLA levels at the highest D-AMPH concentration reached nonspecific binding levels (6.5% of the specific binding), agreeing with results obtained by Chipana et al. (2008). However, the K_i estimated by Chipana was 876 μM, probably reflecting the higher [^{3}H]-MLA concentration (3 nM) that causes a larger Cheng–Prusoff correction.

Following the results from binding experiments, our electrophysiological experiments on primary cultures from the CA1 region demonstrated that a maximal mα7R response could be achieved at the highest ACh concentration (3 mM). This ACh concentration produces a maximal and saturated α7R response in a delivery system similar to ours (Cólon-Saez and Yakel, 2011; personal communication). In contrast to the IC_{50} estimation, the D-AMPH-triggered hyperpolarizing current does affect the normalized inhibition since it appears at the same time as the mα7R response. We found that at 87 and 200 μM D-AMPH, this hyperpolarizing current could at least accounts for 4% and 6% of the total net charge, respectively, causing an "apparent" inhibition of a larger magnitude. Taking that in consideration, the normalized inhibition falls within less than 10% of the maximal response, an inhibition magnitude that has been observed for well-accepted nicotinic and non-nicotinic competitive antagonists, such as α-conotoxin ImI and losartan (Pereira et al., 1996; Vanderheyden et al., 1999).

Aiming to reveal the molecular interactions stabilizing D-AMPH binding, the structural data of an α7/AChBP chimera was selected for *in silico* docking analysis (Li et al., 2011). This chimera presents the highest sequence identity to the α7 nAChR (~64%) and provides the structures for the Apo conformation at high resolution (3.1 Å). The water molecule bridging nicotine to residues Leu104 and Leu116 was included because of the high probability (92% of the time) of finding this water in molecular dynamic simulations (Amiri et al., 2007). Autodock's effectiveness for analyzing nicotinic ligands has been demonstrated by other groups on the AChBP (Brams et al., 2011; Gao et al., 2003).

For D-AMPH, our results suggest that binding is stabilized by hydrogen bonding to the backbone carbonyl group of Ser144, possibly involving a concurrent hydrogen bond with Tyr91's hydroxyl group, and aromatic interactions with the key residues Trp145, Tyr 184, and Tyr191 on the principal side. This implies that hydrogen bonding to nAChR's secondary structure, along with the size of the groups attached to the amine group, may play an important locating role in ligands holding the classical nicotinic pharmacophore. This pharmacophore includes a basic amine at certain distance from a hydrogen bond acceptor (Beers and Reich, 1970; Sheridan et al., 1986). But more importantly, hydrogen bonding to Ser144 may explain D-AMPH's antagonist effects. The hydrogen bond to Ser144 places D-AMPH in a tightly packed location close to the "hinge" created by the B— and C-loops. Steric hindrance at this location, possibly mediated through contacts with the side chains of residues Trp145, Tyr184, and Tyr 192, may prevent C-loop displacement toward the binding pocket, a shift that has been associated with the transition into the open state (Law et al., 2005; Unwin and Fujiyoshi, 2012). Conversely, the classical nicotinic agonists nicotine and epibatidine form hydrogen bonds to Trp145, locating these agonists far from the "hinge" and providing the space to allow C-loop displacement (Celie et al., 2004; Li et al., 2011). The hydrogen bonding preference of these agonists for Trp145 may arise from the steric hindrance provided by the bulky amine groups.

We tested this hypothesis by analyzing a racemic mixture of the chain-extended nicotinoid MPEA through electrophysiology and by docking D-MPEA to the α7/AChBP chimera. Structurally, MPEA is identical to AMPH except for the pyridine ring replacing AMPH's phenyl group, making AMPH acquire the classical nicotinoid pharmacophore. Although the optimal interatomic distance between the amine and the hydrogen bond acceptor in the classical nicotinic pharmacophore is still controversial, the most stable D-MPEA conformation (MM2 minimization: 7.91 kcal/mol; Chem3D 16.0, PerkinElmer Informatics, Inc.) achieves an internitrogen distance of 4.2 Å, which is in close agreement with nicotine's internitrogen distance (4.4 ± 0.1 Å) obtained from Celie's study. Moreover, binding studies analyzing unbranched aminoalkylpyridines similar to MPEA has shown that these compounds bind with a high affinity to the α4β2 nAChR, in the low to middle nanomolar range, and with moderate affinity to the α7 nAChR, in the low micromolar range (De Kloe et al., 2010; Glennon and Dukat, 2000).

(±)-MPEA activates hα7R but with negligible efficacy, supporting our hypothesis that nicotinic ligands capable of forming hydrogen bonds with Ser144 are not effective in activating nAChRs. We ruled out that lack of efficacy is related to the use of a racemic mixture because, as mentioned above, primary amines display lower stereoselectivity on nAChRs. This result also highlights that the classical nicotinoid pharmacophore does not assure agonism on the nAChR, and other factors, such as molecule rigidity and the size of the amine's substituents, should be considered during drug design. Additional electrophysiological studies using aminoalkylpyridines need to be done to provide further evidence about this hypothesis.

Interactions between METH and nAChRs has been associated with physiological responses such as locomotion (Camarasa et al., 2009). In rodents, nAChRs regulate locomotor responses, but previous studies have been mainly focused on β2* nAChRs, which comprise the majority of nicotine binding sites in the nigrostriatal and mesolimbic pathways (Avale et al., 2008; Changeux, 2010; Drenan et al., 2010). Here, we evaluated the role for the α7 nAChR in basal and D-AMPH-induced locomotion.

We selected the use of the α7 nAChR KO mouse line over pharmacological manipulation because, in contrast to in vitro and ex vivo experiments, selective antagonism of the α7 nAChR is difficult to accomplish in in vivo settings. Toxins, such as α-bungarotoxin and α-conotoxin ArIB, do not cross the blood–brain barrier (BBB) and require challenging delivery methods. In the case of MLA, which crosses the BBB, a study has shown that it also blocks α6β2-containing receptors in the striatum, the main brain structure regulating D-AMPH locomotor effects (Mogg et al., 2002; Sharp et al., 1987). The lower (K_i: ~30 nM) but close affinity to α7 nAChRs (K_i: ~1.86 nM) may confound our results due to the uncertainty between drug dose and local brain concentration in molar units (Davies et al., 1999).

On the other hand, results from independent studies have provided evidence supporting the use of α7 nAChR KO mice for studying the role of this receptor on D-AMPH-induced locomotion. This mouse line shows no changes in locomotion in the open-field paradigm and the rotarod (motor coordination), paradigms that requires proper recruitment of the striatum (Paylor et al., 1998; Salas et al., 2007). Our results also agree with the absence of an α7 nAChR-mediated mechanism regulating basal locomotion or open field-related exploratory behavior.

Overall, these results argue against drastic changes in the connectome and physiological functioning of the striatum.

Another risk this mouse line could impose is a functional compensation for the lack of α7 nAChR by other nAChR subtypes, as has been observed in cultures (McGehee et al., 1995). However, this compensation probably cannot substitute the role of α7 nAChRs in neuronal circuitries due to the higher conductance of α7 nAChR for Ca^{2+} ions in comparison to other nAChR subtypes. Following this line, D-AMPH's effects on neurons are Ca^{2+}-sensitive, and the interchange of α7 nAChR for another nAChR could disrupt the intracellular Ca^{2+} signaling required for triggering D-AMPH response (Gnegy et al., 2004). Aligning with this hypothesis, our results displayed a significant reduction in D-AMPH-induced locomotion with respect to the WT; thus, uncovering a possible striatal mechanism that is involved when this brain area is hijacked by D-AMPH.

nAChR upregulation is frequently considered one of the mechanisms leading to nicotine addiction, and it has been suggested that it plays a major role in nicotine locomotor sensitization (Baker et al., 2013). Because D-AMPH also induces sensitization, we tested whether mα7R upregulation is involved in D-AMPH-induced sensitization. In this study, a well-established D-AMPH schedule for inducing sensitization produces no upregulation, ruling out any role of α7 nAChR in AMPH sensitization. Studies have shown that α7 nAChR activation and mRNA synthesis are required for inducing upregulation, contrasting with the pharmacological chaperoning mechanism associated with the β2* nAChRs upregulation (Brown et al., 2013; Peng et al., 1997). This agrees with the D-AMPH antagonist character found in the present study.

The present study raises important questions about the physiological consequences of the AMPH − α7 nAChR interaction. The first question is whether this interaction indeed occurs in vivo. Determination of the effective D-AMPH concentration molarity in the brain interstitial space has been challenging for technical and physiological reasons. Microdialysis has been employed, reporting values of 10 and 200 nM for 2 and 10 mg/kg doses, respectively (Siciliano et al., 2014). However, at the perfusion rate employed in this study (1 μl/min), equilibrium is probably not attained and, because correction for probe efficiency was not reported, is probable that these values are underestimated (Chefer et al., 2009).

Traditionally, blood drug levels have been used as reference, but with the limitation that transport across the BBB may restrain drug access into the brain. METH readily crosses the BBB due to its size, lipophilicity, and membrane translocation through the organic cation transporter OCTN2 (Turowski and Kenny, 2015). METH also evades the BBB efflux pump activity, making its translocation a one-way process and probably causing a higher concentration in the brain. Using decay parameters obtained from a pharmacokinetic study (Hutchaleelaha et al., 1994), a serum D-AMPH concentration of ~25 μM can be estimated 2 min after administration (7.5 mg/kg, i.v.). Because AMPH blood concentrations can achieve micromolar levels at physiological doses and AMPH probably accumulates in the brain, it is plausible that the AMPH − mα7R interaction is an important component of behavioral responses in animal models. Moreover, this interaction could exert a more prominent role during chronic or schedules emulating “binge” administration, which further increase BBB permeability to METH (Turowski and Kenny, 2015).

In humans, pharmacokinetic and pharmacodynamic parameters also suggest that the AMPH − hα7R interaction has physiological consequences. AMPH bioavailability ranges between 70 and 100%, depending on delivery route, and D-AMPH half-life is 10-fold longer in humans than in rodents (~10–11 h vs ~50–70 min, respectively), producing a high and sustained blood concentration (Fuller et al., 1972; Harris et al., 2003; United States Food and Drug Administration, 2017). Blood samples from people detained by the police in Norway and California have reported AMPH and METH concentrations ranging 0.29–11.1 μM with medians of 3.82 and 2.0 μM, respectively (Gustavsen et al., 2006; Melega et al., 2007). It has been estimated that after a single METH dose of 0.26–1 g (typical recreational dose: 250–500 mg) blood concentration reaches 7.5–28.8 μM, and by the fourth intake during binge consumption, blood concentration reaches 17–80 μM (Tallóczy et al., 2008). Single-dose blood concentration levels overlap with the IC_{50} range found in this study. Furthermore, the concentrations during binge consumption are even higher, suggesting the AMPH − hα7R interaction plays a relevant role in the disorders/conditions associated with binging/chronic use.

5. Conclusion

Our results demonstrate that AMPH enantiomers competitively antagonize α7 nAChRs with a potency that may have behavioral consequences, as observed in the open field experiments. Furthermore, our results also provide evidence that the classical nicotinoid pharmacophore does not assure agonistic effects from a molecule. Translating our results into an effective pharmacotherapy will require the identification of which ATS interact with specific nAChR subtypes, the behavioral domains that are affected by these interactions, and the possible benefits of modulating these interactions with proper nAChR pharmacology. Following this idea, preclinical studies has shown that varenicline (an α7 full agonist and partial agonist on β2-containing nAChRs) reduces the positive subjective effect of smoked METH, increases abstinence rates, but has no effect on the reinforcing properties in METH addicts that were not looking for treatment at the beginning of the studies (Brensilver et al., 2013; Verrico et al., 2014).

Funding and disclosure

This study was funded by the National Institutes of Health [grants: 1 R01 GM 098343, 1 P20 GM 103642, 3 P50 NS 038370-13S1, 5 T32 DA 016224, and 5 T32 MH 018870] and Columbia University Summer Undergraduate Research Fellowship (1R01GM098343). The authors declare no conflict of interest.

Acknowledgements

We would like to express our most sincerely gratitude to Dr. David Sulzer for providing materials and equipment for completing this study. We would also like to thank Dr. Jonathan Javitch for his input on result interpretation, Dr. Alexander Sobolevsky for his input on docking analysis, and Ellen Kanter for preparing cellular cultures. J.E.L-O conceived and designed the whole study, performed and analyzed experiments, result interpretation, and wrote the manuscript. D.R.G performed and analyzed cellular experiments, result interpretation, and wrote the manuscript along with J.E.L-O. S.G.R performed immunolabeling experiments. R.M-H. analyzed electrophysiological experiments, provided input for experimental design, and revised the manuscript. M.Q. provided input and equipment for binding experiments. J.A.L-D provided input, materials, and equipment for oocytes experiments and revised the manuscript.

Appendix A. Supplementary data

Supplementary data to this article can be found online at https://doi.org/10.1016/j.neuropharm.2018.10.032.

References

Abreo, M.A., Lin, N.H., Garvey, D.S., Gunn, D.E., Hettinger, A.M., Wasicak, J.T., Pavlik, P.A., Martin, Y.C., Donnelly-Roberts, D.L., Anderson, D.J., Sullivan, J.P., Williams, M., Arneric, S.P., Holladay, M.W., 1996. Novel 3-pyridyl ethers with subnanomolar affinity for central neuronal nicotinic acetylcholine receptors. J. Med. Chem. 39, 817–825. https://doi.org/10.1021/jm9506884.

Alkondon, M., Albuquerque, E.X., 1993. Diversity of nicotinic acetylcholine receptors in rat hippocampal neurons. I. Pharmacological and functional evidence for distinct

structural subtypes. J. Pharmacol. Exp. Therapeut. 265, 1455–1473.
Amiri, S., Sansom, M.S.P., Biggin, P.C., 2007. Molecular dynamics studies of AChBP with nicotine and carbamylcholine: the role of water in the binding pocket. Protein Eng. Des. Sel. 20, 353–359. https://doi.org/10.1093/protein/gzm029.
Avale, M.E., Faure, P., Pons, S., Robledo, P., Deltheil, T., David, D.J., Gardier, A.M., Maldonado, R., Granon, S., Changeux, J.-P., Maskos, U., 2008. Interplay of β2* nicotinic receptors and dopamine pathways in the control of spontaneous locomotion. Proc. Natl. Acad. Sci. U. S. A 105, 15991–15996. https://doi.org/10.1073/pnas.0807635105.
Baker, L.K., Mao, D., Chi, H., Govind, A.P., Vallejo, Y.F., Iacoviello, M., Herrera, S., Cortright, J.J., Green, W.N., Mcgehee, D.S., Vezina, P., 2013. Intermittent nicotine exposure upregulates nAChRs in VTA dopamine neurons and sensitises locomotor responding to the drug. Eur. J. Neurosci. 37, 1004–1011. https://doi.org/10.1111/ejn.12114.
Balster, R.L., Schuster, C.R., 1973. A comparison of *d*-aphetamine, *l*-amphetamine, and methamphetamine self-administration in rhesus monkeys. Pharmacol. Biochem. Behav. 1, 67–71. https://doi.org/10.1016/0091-3057(73)90057-9.
Beers, W.H., Reich, E., 1970. Structure and activity of acetylcholine. Nature 228, 917–922. https://doi.org/10.1038/228917a0.
Brams, M., Pandya, A., Kuzmin, D., van Elk, R., Krijnen, L., Yakel, J.L., Tsetlin, V., Smit, A.B., Ulens, C., 2011. A structural and mutagenic blueprint for molecular recognition of strychnine and d-tubocurarine by different Cys-loop receptors. PLoS Biol. 9, 1–12. https://doi.org/10.1371/journal.pbio.1001034.
Brensilver, M., Heinzerling, K.G., Swanson, A.N., Telesca, D., Furst, B.A., Shoptaw, S.J., 2013. Cigarette smoking as a target for potentiating outcomes for methamphetamine abuse treatment. Drug Alcohol Rev. 32, 96–99. https://doi.org/10.1111/j.1465-3362.2012.00423.x.
Brown, K.C., Perry, H.E., Lau, J.K., Jones, D.V., Pulliam, J.F., Thornhill, B.A., Crabtree, C.M., Luo, H., Chen, Y.C., Dasgupta, P., 2013. Nicotine induces the up-regulation of the α7-nicotinic receptor (α7-nAChR) in human squamous cell lung cancer cells via the Sp1/GATA protein pathway. J. Biol. Chem. 288, 33049–33059. https://doi.org/10.1074/jbc.M113.501601.
Camarasa, J., Ratés, S.G., Pubill, D., Escubedo, E., 2009. The involvement of nicotinic receptor subtypes in the locomotor activity and analgesia induced by methamphetamine in mice. Behav. Pharmacol. 20, 623–630. https://doi.org/10.1097/FBP.0b013e328331ba5b.
Cao, D.-N., Shi, J.-J., Hao, W., Wu, N., Li, J., 2016. Advances and challenges in pharmacotherapies for amphetamine-type stimulants addiction. Eur. J. Pharmacol. 780, 129–135. https://doi.org/10.1016/j.ejphar.2016.03.040.
Celie, P.H.N., Van Rossum-Fikkert, S.E., Van Dijk, W.J., Brejc, K., Smit, A.B., Sixma, T.K., 2004. Nicotine and carbamylcholine binding to nicotinic acetylcholine receptors as studied in AChBP crystal structures. Neuron 41, 907–914. https://doi.org/10.1016/S0896-6273(04)00115-1.
Center for Behavioral Health Statistics and Quality, 2017. 2016 National Survey on Drug Use and Health: Detailed Tables. Substance Abuse and Mental Health Services Administration, Rockville, MD.
Changeux, J.-P., 2010. Nicotine addiction and nicotinic receptors: lessons from genetically modified mice. Nat. Rev. Neurosci. 11, 389–401. https://doi.org/10.1038/nrn2849.
Chefer, V.I., Thompson, A.C., Zapata, A., Shippenberg, T.S., 2009. Overview of brain microdialysis. In: Current Protocols in Neuroscience. John Wiley & Sons, Inc., Hoboken, NJ, USA, pp. 1–28. https://doi.org/10.1002/0471142301.ns0701s47.
Chipana, C., García-Ratés, S., Camarasa, J., Pubill, D., Escubedo, E., 2008. Different oxidative profile and nicotinic receptor interaction of amphetamine and 3,4-methylenedioxy-methamphetamine. Neurochem. Int. 52, 401–410. https://doi.org/10.1016/j.neuint.2007.07.016.
Cólon-Sáez, J.O., Yakel, J.L., 2011. The α7 nicotinic acetylcholine receptor function in hippocampal neurons is regulated by the lipid composition of the plasma membrane. J. Physiol. 589, 3163–3174. https://doi.org/10.1113/jphysiol.2011.209494.
Copeland, J.R., Adem, A., Jacob, P., Nordberg, A., 1991. A comparison of the binding of nicotine and nornicotine stereoisomers to nicotinic binding sites in rat brain cortex. Naunyn-Schmiedeberg's Arch. Pharmacol. 343, 123–127.
Davies, A.R.L., Hardick, D.J., Blagbrough, I.S., Potter, B.V.L., Wolstenholme, A.J., Wonnacott, S., 1999. Characterisation of the binding of [^{3}H]methyllycaconitine: a new radioligand for labelling α7-type neuronal nicotinic acetylcholine receptors. Neuropharmacology 38, 679–690.
De Kloe, G.E., Retra, K., Geitmann, M., Källblad, P., Nahar, T., Van Elk, R., Smit, A.B., Van Muijlwijk-Koezen, J.E., Leurs, R., Irth, H., Danielson, U.H., De Esch, I.J.P., 2010. Surface plasmon resonance biosensor based fragment screening using acetylcholine binding protein identifies ligand efficiency hot spots (le hot spots) by deconstruction of nicotinic acetylcholine receptor α7 ligands. J. Med. Chem. 53, 7192–7201. https://doi.org/10.1021/jm100834y.
Drenan, R.M., Grady, S.R., Steele, A.D., Mckinney, S., Patzlaff, N.E., Mcintosh, J.M., Marks, M.J., Miwa, J.M., Lester, H.A., 2010. Cholinergic modulation of locomotion and striatal dopamine release is mediated by α6α4 * nicotinic acetylcholine receptors. J. Neurosci. 30, 9877–9889. https://doi.org/10.1523/JNEUROSCI.2056-10.2010.
Elkashef, A.M., Rawson, R.A., Anderson, A.L., Li, S.-H., Holmes, T., Smith, E.V., Chiang, N., Kahn, R., Vocci, F., Ling, W., Pearce, V.J., McCann, M., Campbell, J., Gorodetzky, C., Haning, W., Carlton, B., Mawhinney, J., Weis, D., 2008. Bupropion for the treatment of methamphetamine dependence. Neuropsychopharmacology 33, 1162–1170. https://doi.org/10.1038/sj.npp.1301481.
Fuller, R.W., Molloy, B.B., Roush, B.W., Hauser, K.M., 1972. Disposition and behavioral effects of amphetamine and β,β-difluoroamphetamine in mice. Biochem. Pharmacol. 21, 1299–1307.
Gao, F., Bern, N., Little, A., Wang, H.-L., Hansen, S.B., Talley, T.T., Taylor, P., Sine, S.M., 2003. Curariform antagonists bind in different orientations to acetylcholine-binding protein. J. Biol. Chem. 278, 23020–23026. https://doi.org/10.1074/jbc.M301151200.
Glennon, R.A., Dukat, M., 2000. Central nicotinic receptor ligands and pharmacophores. Pharm. Acta Helv. 74, 103–114. https://doi.org/10.1016/S0165-7208(00)80006-9.
Gnegy, M.E., Khoshbouei, H., Berg, K.A., Javitch, J.A., Clarke, W.P., Zhang, M., Galli, A., 2004. Intracellular Ca^{2+} regulates amphetamine-induced dopamine efflux and currents mediated by the human dopamine transporter. Mol. Pharmacol. 66, 137–143. https://doi.org/10.1124/mol.66.1.137.
Guo, X., Lester, R.A.J., 2007. Regulation of nicotinic acetylcholine receptor desensitization by Ca2+. J. Neurophysiol. 97, 93–101. https://doi.org/10.1152/jn.01047.2005.
Gustavsen, I., Mørland, J., Bramness, J.G., 2006. Impairment related to blood amphetamine and/or methamphetamine concentrations in suspected drugged drivers. Accid. Anal. Prev. 38, 490–495. https://doi.org/10.1016/j.aap.2005.11.005.
Hall, D.A., Stanis, J.J., Marquez Avila, H., Gulley, J.M., 2008. A comparison of amphetamine- and methamphetamine-induced locomotor activity in rats: evidence for qualitative differences in behavior. Psychopharmacology 195, 469–478. https://doi.org/10.1007/s00213-007-0923-8.
Harris, D.S., Boxenbaum, H., Everhart, E.T., Sequeira, G., Mendelson, J.E., Jones, R.T., 2003. The bioavailability of intranasal and smoked methamphetamine. Clin. Pharmacol. Ther. 74, 475–486. https://doi.org/10.1016/j.clpt.2003.08.002.
Hénault, C.M., Sun, J., Therien, J.P.D., DaCosta, C.J.B., Carswell, C.L., Labriola, J.M., Juranka, P.F., Baenziger, J.E., 2015. The role of the M4 lipid-sensor in the folding, trafficking, and allosteric modulation of nicotinic acetylcholine receptors. Neuropharmacology 96, 157–168. https://doi.org/10.1016/j.neuropharm.2014.11.011.
Huganir, R.L., Delcour, A.H., Greengard, P., Hess, G.P., 1986. Phosphorylation of the nicotinic acetylcholine receptor regulates its rate of desensitization. Nature 321, 774–776. https://doi.org/10.1038/321774a0.
Hutchaleelaha, A., Sukbuntherng, J., Chow, H.-H., Mayersohn, M., 1994. Disposition kinetics of d-and l-amphetamine following intravenous administration of racemic amphetamine to rats. Drug Metab. Dispos. 22, 406–411.
Lamb, R.J., Henningfield, J.E., 1994. Human d-amphetamine drug discrimination: methamphetamine and hydromorphone. J. Exp. Anal. Behav. 61, 169–180.
Law, R.J., Henchman, R.H., McCammon, J.A., 2005. A gating mechanism proposed from a simulation of a human 7 nicotinic acetylcholine receptor. Proc. Natl. Acad. Sci. U. S. A 102, 6813–6818. https://doi.org/10.1073/pnas.0407739102.
Li, S., Huang, S., Bren, N., Noridomi, K., Dellisanti, C.D., Sine, S.M., Chen, L., 2011. Ligand-binding domain of an α7-nicotinic receptor chimera and its complex with agonist. Nat. Neurosci. 14, 1253–1259. https://doi.org/10.1038/nn.2908.
Liu, P.S., Liaw, C.T., Lin, M.K., Shin, S.H., Kao, L.S., Lin, L.F., 2003. Amphetamine enhances Ca2+ entry and catecholamine release via nicotinic receptor activation in bovine adrenal chromaffin cells. Eur. J. Pharmacol. 460, 9–17. https://doi.org/10.1016/S0014-2999(02)02870-4.
Lopez-Hernandez, G., Placzek, A.N., Thinschmidt, J.S., Lestage, P., Trocme-Thibierge, C., Morain, P., Papke, R.L., 2007. Partial agonist and neuromodulatory activity of S 24795 for alpha7 nAChR responses of hippocampal interneurons. Neuropharmacology 53, 134–144. https://doi.org/10.1016/j.neuropharm.2007.04.007.
McGehee, D.S., Heath, M.J., Gelber, S., Devay, P., Role, L.W., 1995. Nicotine enhancement of fast excitatory synaptic transmission in CNS by presynaptic receptors. Science 269, 1692–1696. https://doi.org/10.1126/science.7569895.
Melega, W.P., Cho, A.K., Harvey, D., Lacan, G., 2007. Methamphetamine blood concentrations in human abusers: application to pharmacokinetic modeling. Synapse 61, 216–220. https://doi.org/10.1002/syn.20365.
Melega, W.P., Williams, A.E., Schmitz, D.A., DiStefano, E.W., Cho, A.K., 1995. Pharmacokinetic and pharmacodynamic analysis of the actions of D-amphetamine and D-methamphetamine on the dopamine terminal. J. Pharmacol. Exp. Therapeut. 274, 90–96.
Miech, R.A., Johnston, L.D., O'Malley, P.M., Bachman, J.G., Schulenberg, J.E., Patrick, M.E., 2017. Monitoring the Future: National Survey Results on Drug Use, 1975-2016: Volume I, Secondary School Students. Institute for Social Research, The University of Michigan, Ann Arbor, MI, pp. 1–683.
Mogg, A.J., Whiteaker, P., McIntosh, J.M., Marks, M., Collins, A.C., Wonnacott, S., 2002. Methyllycaconitine is a potent antagonist of α-conotoxin-MII-sensitive presynaptic nicotinic acetylcholine receptors in rat striatum. J. Pharmacol. Exp. Therapeut. 302, 197–204. https://doi.org/10.1124/jpet.302.1.197.
Musso, D.L., Mehta, N.B., Soroko, F.E., Ferris, R.M., Hollingsworth, E.B., Kenney, B.T., 1993. Synthesis and evaluation of the antidepressant activity of the enantiomers of bupropion. Chirality 5, 495–500. https://doi.org/10.1002/chir.530050704.
Palma, E., Bertrand, S., Binzoni, T., Bertrand, D., 1996. Neuronal nicotinic alpha 7 receptor expressed in Xenopus oocytes presents five putative binding sites for methyllycaconitine. J. Physiol. 491, 151–161.
Paylor, R., Nguyen, M., Crawley, J.N., Patrick, J., Beaudet, A., Orr-Urtreger, A., 1998. α7 nicotinic receptor subunits are not necessary for hippocampal-dependent learning or sensorimotor gating: a behavioral characterization of acra7-deficient mice. Learn. Mem. 5, 302–316.
Peng, X., Gerzanich, V., Anand, R., Wang, F., Lindstrom, J., 1997. Chronic nicotine treatment up-regulates α3 and α7 acetylcholine receptor subtypes expressed by the human neuroblastoma cell line SH-SY5Y. Mol. Pharmacol. 51, 776–784.
Pereira, E.F.R., Alkondon, M., McIntosh, J.M., Albuquerque, E.X., 1996. α-Conotoxin-ImI: a competitive antagonist at α-bungarotoxin-sensitive neuronal nicotinic receptors in hippocampal neurons. J. Pharmacol. Exp. Therapeut. 278, 1472–1483.
Salas, R., Main, A., Gangitano, D., De Biasi, M., 2007. Decreased withdrawal symptoms but normal tolerance to nicotine in mice null for the α7 nicotinic acetylcholine receptor subunit. Neuropharmacology 53, 863–869. https://doi.org/10.1016/j.

neuropharm.2007.08.017.
Sharp, T., Zetterström, T., Ljungberg, T., Ungerstedt, U., 1987. A direct comparison of amphetamine-induced behaviours and regional brain dopamine release in the rat using intracerebral dialysis. Brain Res. 401, 322–330.
Schulenberg, J.E., Johnston, L.D., O'Malley, P.M., Bachman, J.G., Miech, R.A., Patrick, M.E., 2017. Monitoring the Future: National Survey Results on Drug Use, 1975-2016: Volume II, College Students and Adults Ages 19-55. Institute for Social Research, The University of Michigan, Ann Arbor, MI.
Sheridan, R.P., Nilakantan, R., Dixon, J.S., Venkataraghavan, R., 1986. The ensemble approach to distance geometry: application to the nicotinic pharmacophore. J. Med. Chem. 29, 899–906.
Siciliano, C. a, Calipari, E.S., Ferris, M.J., Jones, S.R., 2014. Biphasic mechanisms of amphetamine action at the dopamine terminal. J. Neurosci. 34, 5575–5582. https://doi.org/10.1523/JNEUROSCI.4050-13.2014.
Sitte, H.H., Freissmuth, M., 2015. Amphetamines, new psychoactive drugs and the monoamine transporter cycle. Trends Pharmacol. Sci. 36, 41–50. https://doi.org/10.1016/j.tips.2014.11.006.
Slemmer, J.E., Martin, B.R., Damaj, M.I., 2000. Bupropion is a nicotinic antagonist. J. Pharmacol. Exp. Therapeut. 295, 321–327.
Spitzmaul, G.F., Esandi, M.C., Bouzat, C., 1999. Amphetamine acts as a channel blocker of the acetylcholine receptor. Neuroreport 10, 2175–2181.
Sulzer, D., Sonders, M.S., Poulsen, N.W., Galli, A., 2005. Mechanisms of neurotransmitter release by amphetamines: a review. Prog. Neurobiol. 75, 406–433. https://doi.org/10.1371/journal.ppat.0040028.
Tallóczy, Z., Martinez, J., Joset, D., Ray, Y., Gácser, A., Toussi, S., Mizushima, N., Nosanchuk, J., Goldstein, H., Loike, J., Sulzer, D., Santambrogio, L., 2008. Methamphetamine inhibits antigen processing, presentation, and phagocytosis. PLoS Pathog. 4, 1–11. https://doi.org/10.1371/journal.ppat.0040028.
Turowski, P., Kenny, B.A., 2015. The blood-brain barrier and methamphetamine: open sesame? Front. Neurosci. 9, 1–7. https://doi.org/10.3389/fnins.2015.00156.
United Nations Office on Drugs and Crime, 2016. World Drug Report. United Nation publications, Vienna Sales No. E.16.XI.7.
United States Food and Drug Administration, 2017. Adderall CII. [WWW Document]. Adderall CII. http://www.accessdata.fda.gov/drugsatfda_docs/label/2017/011522s043lbl.pdf.
Unwin, N., Fujiyoshi, Y., 2012. Gating movement of acetylcholine receptor caught by plunge-freezing. J. Mol. Biol. 422, 617–634. https://doi.org/10.1016/j.jmb.2012.07.010.
Vanderheyden, P.M.L., Fierens, F.L.P., De Backer, J.P., Fraeyman, N., Vauquelin, G., 1999. Distinction between surmountable and insurmountable selective AT 1 receptor antagonists by use of CHO-K1 cells expressing human angiotensin II AT 1 receptors. Br. J. Pharmacol. 126, 1057–1065.
Verrico, C.D., Mahoney, J.J., Thompson-Lake, D.G.Y., Bennett, R.S., Newton, T.F., De La Garza, R., 2014. Safety and efficacy of varenicline to reduce positive subjective effects produced by methamphetamine in methamphetamine-dependent volunteers. Int. J. Neuropsychopharmacol. 17, 223–233. https://doi.org/10.1017/S146114571300134X.
Winters, K.C., Tanner-Smith, E.E., Bresani, E., Meyers, K., 2014. Current advances in the treatment of adolescent drug use. Adolesc. Health Med. Ther. 5, 199–210. https://doi.org/10.2147/AHMT.S48053.